Edelweiss Applied Science and Technology
ISSN: 2576-8484
Vol. 10, No. 1, 102-127
2026
Publisher: Learning Gate
DOI: 10.55214/2576-8484.v10i1.11532

Evaluation of the ethanolic extract of *Mondai whitei (Hook.f.)* Skeels for their antioxidant, anti-inflammatory and antidiabetic properties

Mojisola Abosede Bayode[1*], Akingbolabo D. Ogunlakin[1], Gideon Ampompa Gyebi[2], Oluwafemi Adeleke Ojo[1,3*]
[1]Department of Biochemistry, Bowen University, Iwo, Nigeria; mojisola.bayode@bowen.edu.ng (M.A.B.) oluwafemiadeleke08@gmail.com (O.A.O.).
[2]Department of Biotechnology and Food Science, Faculty of Applied Sciences, Durban University of Technology, Durban, 4000, South Africa.
[3]Research Centre for Integrative Physiology and Pharmacology, Institute of Biomedicine, University of Turku, Turku, 20014, Finland.

Abstract: This research evaluated the antidiabetic, antioxidant, and anti-inflammatory properties and phytochemical profile of the ethanolic extract from Mondai whitei roots via in silico, ex vivo, and in vitro approaches. The antioxidant activity (ferric-reducing power; DPPH radical scavenging, catalase, lipid peroxidation, and superoxide dismutase), antidiabetic activity (α-glucosidase and α-amylase inhibition), and anti-inflammatory effects (protein denaturation, proteinase inhibition, and membrane stabilization) were determined via in vitro tests. Ex vivo, liver homogenate was exposed to $FeSO_4$-induced oxidative stress and treated with graded concentrations of the extract. The extract scavenged DPPH in a concentration-dependent manner and exhibited greater reducing power than ascorbic acid at 200 µg/mL. In $FeSO_4$-treated tissue, the extract restored oxidative stress markers (malondialdehyde, SOD, and catalase) toward baseline, indicating protection against lipid peroxidation. The extract inhibited α-amylase (IC_{50} = 81.597 ± 0.776 mg/mL) and α-glucosidase, and demonstrated anti-inflammatory effects via the inhibition of protein denaturation, membrane stabilization, and proteinase inhibition (IC_{50} = 58.715 ± 1.996 µg/mL). HPLC identified seventeen compounds, with 2-chloro-4-methoxybenzaldehyde and vanillin being the most abundant. In silico docking of these constituents against α-glucosidase revealed that α-amylase, dipeptidyl peptidase IV strongly predicted the binding of chloropropacin, propacin, and yohimbine. Collectively, these findings suggest that the antidiabetic, antioxidant, and anti-inflammatory properties of M. whitei arise from its secondary metabolites, highlighting the role of the extract and its constituents as potential leads for managing diabetes and oxidative-stress–related inflammation.

Keywords: *Antidiabetic, Anti-inflammatory, Antioxidant, Computational models, Mondia whitei, Phytochemicals.*

1. Introduction

The metabolic disease known as diabetes mellitus (DM) is characterized by elevated blood glucose levels caused by either an insufficient amount of insulin or insulin dysfunction [1]. People who have diabetes typically experience incalculable suffering and debilitating complications that might result in morbidity and death [2]. According to the International Diabetes Federation, 366 million people were predicted to have diabetes mellitus in 2011; that number will increase to 552 million by 2030. Every nation is seeing an increase in the number of persons with type 2 diabetes, with 80% of those affected residing in low- and middle-income nations [3]. There is an urgent need to find efficient treatment methods because of the elevated occurrence rate and crippling side effects. Hyperglycemia-induced oxidative stress, which manifests as increased production of reactive oxygen/nitrogen species

History: Received: 14 October 2025; Revised: 1 December 2025; Accepted: 4 December 2025; Published: 1 January 2026
* Correspondence: mojisola.bayode@bowen.edu.ng

(ROS/RNS) and inhibition of antioxidant defenses, such as those of glutathione peroxidase (GPx), catalase (CAT), and superoxide dismutase (SOD), has a major impact on the pathophysiology of diabetes mellitus [4]. Owing to this imbalance in ROS/RNS and antioxidant defense mechanisms, tissues may become more susceptible to oxidative stress, which exacerbates the consequences of diabetes mellitus [5].

Oxidative stress and inflammation play major roles in the development of DM [6]. The immune system's protective response to infection or tissue injury is inflammation, whereas oxidative stress results from an imbalance between the body's antioxidant system and the production of reactive oxygen species (ROS). One of the most prevalent risk factors for diabetes mellitus is hyperglycemia [7, 8]. High blood glucose levels in hyperglycemic patients trigger inflammatory pathways that increase the synthesis of adipokines, chemokines, and proinflammatory cytokines, which attract immune cells to the kidneys [9]. Reactive intermediates produced by neutrophils and monocytes aid in the generation of ROS, which cause oxidative stress and kidney injury [10]. Furthermore, high glucose levels trigger the polyol pathway, which results in the production of sorbitol, leading to oxidative stress and exacerbating inflammation [11].

Reactive oxygen species (ROS) are naturally occurring byproducts of oxygen consumption in the mitochondria and other cellular functions under normal physiological conditions [12]. ROS play crucial roles in muscle power control, apoptosis, gene expression, cell signaling, and cell differentiation at low concentrations [13, 14]. ROS include free radicals such as nitrogen oxide ($NO^{\bullet}$), hydroxyl radicals ($^{\bullet}OH$), superoxide ($O_2^{\bullet-}$), singlet oxygen ($^1O_2$), and hydrogen peroxide (H_2O_2) [15]. They are produced naturally by biological processes in organelles, including mitochondria; peroxisome-based enzymes such as urate oxidase and acyl-CoA oxidases [16]; and endoplasmic reticulum-based enzymes such as cytochrome P-450, B5 enzymes, and diamine oxidase [17]. Environmental factors such as pollutants, radiation, food, and drugs can produce exogenous ROS [18].

2. Materials and Methods

2.1. Plant Material and Preparation of Ethanolic Extract of Mondai Whitei Roots

Mondai whitei dry roots were obtained from a local market (Odori) in Iwo, Osun State, Nigeria, and then authenticated at Bowen University Herbarium. A voucher sample (BUH:099) was deposited at the institution. The roots were cut into pieces to increase their surface area, air-dried, and subsequently blended into a fine powder with an electronic blending machine. The powdered sample was used for the extraction process.

2.2. In vitro Antioxidants

2.2.1. 2,2-Diphenyl-1-Picrylhydrazyl (DPPH) Radical Scavenging Activity

The antioxidant activity of the extracts, based on their ability to scavenge DPPH radicals, was assessed following the method described by Ojo et al. [19]. Ascorbic acid was used as the reference standard for comparison. The percentage inhibition of DPPH radicals was calculated using the following formula:

$$\%\text{DPPH} = \frac{\text{Abs}_{\text{control}} - \text{Abs}_{\text{sample}} \times 100}{\text{Abs}_{\text{control}}}$$

2.2.2. Ferric Reducing Antioxidant Power (FRAP) Assay

The ferric ion reducing capacity of *Mondia whitei* extract was evaluated following the methods described by Ojo et al. [19] and Ahmad et al. [20] with slight modifications. The absorbance was measured at 593 nm, and the results are expressed as µmol of Fe(II) per gram of dry powder weight, and an $FeSO_4$ standard calibration curve was used for quantification.

Edelweiss Applied Science and Technology
ISSN: 2576-8484
Vol. 10, No. 1: 102-127, 2026
DOI: 10.55214/2576-8484.v10i1.11532

2.3. Ex Vivo Analysis

2.3.1. Experimental Animals and Organ Preparation

Four healthy male Wistar rats weighing 250–300 g each were purchased from the Department of Biochemistry, University of Ilorin, Ilorin, Nigeria. The rats were euthanized with halothane after being fasted for the previous night, and their livers were then removed and homogenized in 1% Triton X-100 added to 50 mM phosphate buffer. The homogenate was subsequently centrifuged at 15,000 rpm and 40°C. For *ex vivo* research, the supernatants were collected in simple plain tubes. With a few minor modifications, the methods described below were used to induce liver injury *ex vivo*. In brief, 200 µL of the organ supernatant comprising various concentrations (30–240 µg/mL) of plant extract mixtures was combined with 100 µL of 0.1 mM $FeSO_4$. After incubation for 30 min at 37°C, the samples were then used for biochemical analyses. The normal control used reaction mixtures with only the organ supernatant, and the negative control used reaction mixtures with only the tissue supernatant and $FeSO_4$.

2.3.2. Catalase (CAT) Activity

This was determined with slight modifications to the procedure described by Ojo et al. [19]. S780 µL of 50 mM phosphate buffer and 300 µL of 2 M H_2O_2 were added to various concentrations of tissue samples extracted with methanol. Absorbance at 240 nm was measured at 1-minute intervals, with readings taken every three minutes.

2.3.3. Superoxide Dismutase (SOD)

SOD activity was evaluated as described previously [21]. In brief, diethylenetriaminepentaacetic acid (170 µL) and incubated sample (15 µL) were added together in a test tube. Then, 6-hydroxydopamine (15 µL) was added to the mixture, which was gently mixed by shaking. The mixture was finally incubated at 492 nm every 3 minutes at 1-minute intervals.

2.3.4. Malondialdehyde Level Determination

The procedure described by McIntyre et al. [22] was used to evaluate the capacity of the extract to inhibit malondialdehyde. This was done by taking 100 µL of tissue lysates that contained different concentrations of the extract. Then, 1000 µL of 0.25% thiobarbituric acid, 100 µL of 8.1% SDS, and 375 µL of 20% acetic acid were added. At 95°C, the mixture was boiled for one hour in a water bath. The mixture was then allowed to cool to room temperature, and the absorbance at 532 nm was measured.

2.4. In vitro Anti-inflammatory Test

2.4.1. Erythrocyte Membrane Stabilization

HRBC membrane stabilization was measured via the procedure reported by Hogan et al. [23]. In brief, 2 mL mixtures were prepared by mixing different concentrations of the extract and a 10% suspension of red blood cells containing the standard diclofenac drug. The mixtures were kept at 56°C in the oven for 30 minutes. Afterwards, the samples were centrifuged at 2500 revolutions per minute (rpm) for 5 minutes. The supernatant was then read at a wavelength of 560 nm.

2.4.2. Inhibition of Protein Denaturation

The method described by Hogan et al. [23] was used to evaluate the inhibition of protein denaturation. The samples included varying amounts of the extract and/or standard diclofenac, with 10 µL of 1% bovine serum albumin solution. These samples were heated to 55°C for 30 minutes and allowed to cool, after which the 660 nm wavelength was read. The percentage of inhibition was calculated as the degree to which protein denaturation was prevented.

Edelweiss Applied Science and Technology
ISSN: 2576-8484
Vol. 10, No. 1: 102-127, 2026
DOI: 10.55214/2576-8484.v10i1.11532

2.4.3. Proteinase Inhibitory Assay

This was accomplished via the method described by Hogan et al. [23]. One milliliter of the extract was mixed with 2 mL of Tris-HCl buffer and 0.06 mg of trypsin and incubated for 5 minutes at 37°C. Afterwards, 0.8% (w/v) casein was added to the mixture, which was subsequently incubated for 20 minutes. The reaction was stopped by the addition of 2 mL of 70% perchloric acid. The absorbance of the resulting mixture was measured at 210 nm following centrifugation.

2.5. Antidiabetic Assays on Mondai Whitei Extract

2.5.1. In vitro evaluation of α-amylase inhibition

This was accomplished via the method described by Ahmad et al. [20]. A fresh enzyme preparation consisting of 5 units per milliliter in pH 6.7 ice-cold PBS with a concentration of 20 mM and containing 6.7 mM NaCl was prepared. A 250-µL aliquot of the enzyme was mixed with inhibitors (*Mondai whitei* extract or acarbose) at different concentrations (blank samples were not included), followed by a 20-minute incubation period at 37°C. A 0.5% (w/v) starch mixture was added to the mixture, which was subsequently incubated for an additional 15 minutes at 37°C. Immediately after adding the DNS reagent, the mixture was heated to 100°C for 10 minutes. The absorbance was measured at 540 nm. All experiments were carried out in triplicate, and the percent α-amylase inhibitory activity was calculated according to the following formula:

$$\text{Inhibition percentage} = \frac{Abs\ of\ control - Abs\ of\ sample}{Abs\ of\ control} \times 100$$

2.5.2. Inhibition of α-Glucosidase Activity

The impact of *M. whitei* extract on intestinal α-glucosidase activity was assessed via the method outlined by Bouslamti et al. [24], which measures the amount of glucose produced from sucrose hydrolysis. The assay mixture consisted of 100 µl of 50 mM sucrose, 1000 µl of 50 mM phosphate buffer (pH = 7.5), and 100 µl of α-glycosidase enzyme solution (10 I.U.). This mixture was supplemented with different amounts of *Mondai whitei* extract, distilled water (control), or acarbose as a positive control. The absorbance of the final solution was then determined at a wavelength of 500 nm.

2.6. Computational Analysis of High-Performance Liquid Chromatography (HPLC)-Identified Compounds Targeting α-Amylase, Dipeptidyl Peptidase IV (DPP IV), and α-Glucosidase Enzymes

2.6.1. Ligand Preparation

The structural data (SDF) for the identified HPLC compounds and reference compounds were retrieved from PubChem and loaded into PyRx-Python 0.8's Open Babel module [25]. The secondary metabolites underwent energy minimization via Open Babel using the universal force field (UFF) and conjugate gradient descent optimization, after which they were converted to pdbqt format to prepare for docking analysis.

2.6.2. Retrieval and Processing of Protein Targets

The native ligand acarbose was attached to the 3D structures of human pancreatic alpha-amylase at the active site (PDB ID: 1B2Y; resolution: 3.20 Å; amino acid sequence length: 496) [26] and human glucosidase (PDB ID: 3TOP; resolution: 2.88 Å; amino acid sequence length: 908) complexes with acarbose and DPP4 (PDB ID: 6B1E; resolution: 1.77 Å; Vildagliptin 6B1E complexes with amino acid sequence length: 908) were obtained from the Protein Data Bank (http://www.rcsb.org). Using MGL AutoDockTools, the cocrystallized ligand and water molecules were eliminated to prepare the proteins [27].

Edelweiss Applied Science and Technology
ISSN: 2576-8484
Vol. 10, No. 1: 102-127, 2026
DOI: 10.55214/2576-8484.v10i1.11532

2.6.3. Molecular Docking

Using PyRx-Python Prescription 0.8 (https://pyrx.sourceforge.io/) and the AutoDock Vina module [28], the identified compounds and reference standards (vildagliptin and acarbose) were docked into the protein active sites. The ligand count in PyRx 0.8 was reduced and imported via Open Babel. Before the docking analysis, the ligands were minimized using the universal force field (UFF), and conjugate gradient descent was employed as the optimization technique. By mapping the area around the catalytic and interacting residues with the cocrystallized compounds, the secondary metabolites and acarbose were docked into the binding site of human pancreatic alpha-amylase using the grid box dimensions obtained from the previously validated docking procedure.

2.7. Ensemble-Based Docking Simulation of the Unbound Proteins via Molecular Dynamics

Molecular dynamics simulations were performed on the top two compounds that had the greatest docking scores against the target (α-amylase). The complexes of the top two compounds and reference compounds were run through an all-atom molecular dynamics (MD) simulation with GROMACS 2019.2 for 100 nanoseconds using the GROMOS96 43a1 force field [29, 30]

The topological parameters of ions, water molecules, and protein amino acids were determined using the CHARMM36m force field [31], whereas the ligand molecules were parameterized using the CHARMM General Force Field (CGenFF) tool of CHARMM-GUI [32]. By using the V-rescale method, the temperature was increased to 310 K while maintaining an atmospheric pressure of 1 atm via a Berendsen barostat.

2.7.1. Postmolecular Analysis of Dynamics Simulation

After that, the outcomes of the 100 ns MD simulation were plotted and examined. VMD scripts were used to analyze the MD simulation trajectories and calculate the radius of gyration (ROG), solvent-accessible surface area (SASA), number of H-bonds, root mean square deviation (RMSD), and root mean square fluctuation (RMSF) [33]. Origin v 6.0 Deschenes and David A. Vanden Bout University of Texas 2000 was used to plot the generated data. The binding free energy (BFE) of the top-ranked secondary metabolites was determined via the Molecular Mechanics Generalized Born Surface Area (MM/GBSA) method implemented in gmx_MMPBSA within the GROMACS 2019.2 package [34, 35]. The standard formula $\Delta G_{bind} = G_{complex} - (G_{receptor} + G_{ligand})$ was used to calculate the BFE via the complete snapshots taken from the 100 ns trajectories. Energy derived from residues via the "idecomp = 1" option was used to perform the computations. The energy was further broken down into van der Waals, electrostatic energy, polar, and SAS components of the GB terms via the "idecomp = 2" option [36, 37]. The crucial amino acid residues involved in binding were identified by examining each amino acid's energy contributions after the breakdown analysis was completed.

2.8. ADMET Analysis and in silico Drug Likeness of the Most Highly Ranked Natural Compounds

The top two compounds with strong docking scores were subjected to rigorous in silico evaluation to assess their drug-likeness and ADMET profiles. For drug-likeness, the SwissADME platform (http://www.swissadme.ch/index.php) was used by applying filters such as Verber, Ghose, Egan, and Lipinski. Moreover, the SuperPred webserver (http://lmmd.ecust.edu.cn/admetsar1/predict/) helps predict their absorption, distribution, metabolism, excretion, and Tox (ADME/Tox) characteristics, providing a comprehensive view of their potential as drug candidates.

2.9. Statistical Analysis

GraphPad Prism version 7 was used to analyze the data statistically via one-way ANOVA and multiple t tests. The results are shown as means ± standard deviations. Significant differences between the control and treated groups, as well as among several treatment groups, were assessed using 95% confidence intervals.

Edelweiss Applied Science and Technology
ISSN: 2576-8484
Vol. 10, No. 1: 102-127, 2026
DOI: 10.55214/2576-8484.v10i1.11532

3. Results

3.1. Antioxidant activity

The antioxidant properties of the ethanolic extract of Mondai whitei were evaluated via two assays. The ability of *Mondai whitei* extract to scavenge 2,2-diphenyl-1-picrylhydrazyl (DPPH) radicals increased in a concentration-dependent manner (Figure 1a). Similar trends were observed for the DPPH activity of ascorbic acid. However, the extract exhibited greater scavenging ability at the same concentration than did ascorbic acid. To further validate the antioxidant power of *Mondai whitei*, at the maximum concentration, an assay for ferric reducing antioxidant power (FRAP) was performed at the highest concentration used in the DPPH assay (200 µg/mL). *M. whitei* demonstrated greater antioxidant power because more Fe^{2+} was released than with ascorbic acid.

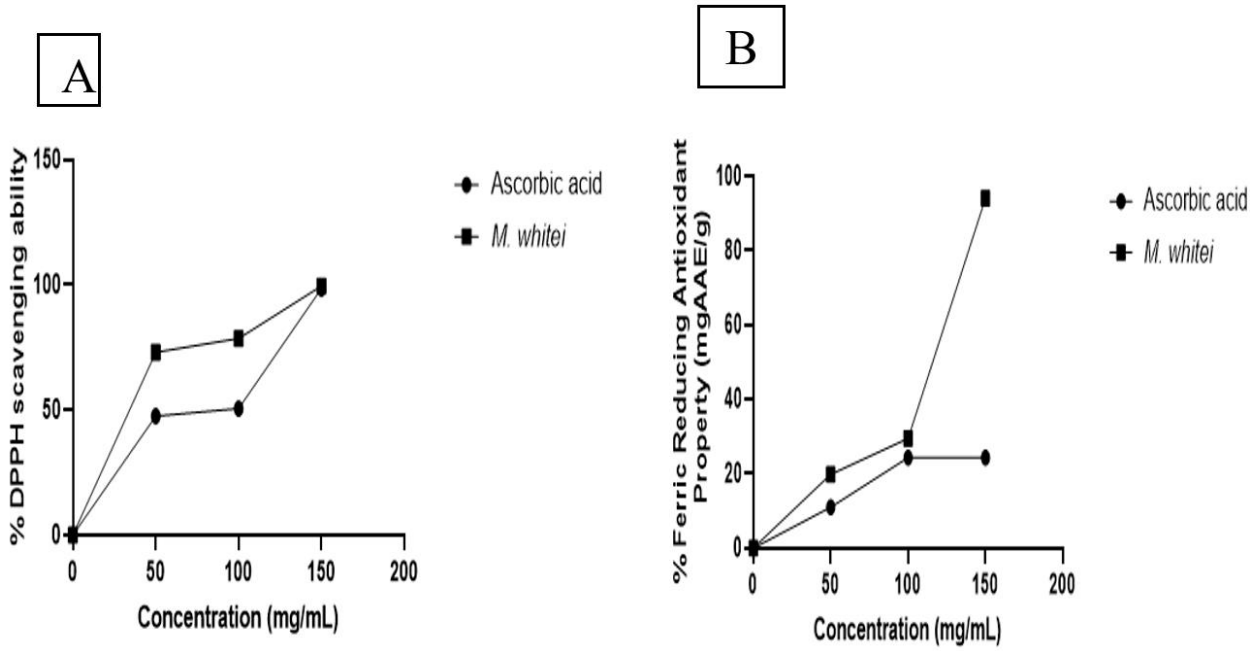

Figure 1.
DPPH radical scavenging ability (A) and ferric reducing antioxidant power (B) of the ethanolic extract of *Mondai whitei* roots.

3.2. Ex vivo Antioxidant Analysis

CAT activity was significantly (p=0.05) reduced in the liver tissue of rats treated with $FeSO_4$. CAT activity was considerably elevated by the *Mondai Whitei* extract ($p < 0.05$), with the greatest effect observed in the 1000 µg/mL group. SOD activity in the liver tissues of the rats exposed to $FeSO_4$ was significantly reduced ($p < 0.05$) (Figure 2b). The dose-dependent increase in SOD activity caused by the *Mondai Whitei* extract was similar to that observed in the normal group ($p < 0.05$). The malondialdehyde level in the $FeSO_4$-treated rats was notably elevated (Figure 2c). Conversely, treatment with *M. Whitei* extract led to a significant ($p < 0.05$) decrease in malondialdehyde levels, which was close to normal, with the 1000 µg/mL dose having the most pronounced effect.

Edelweiss Applied Science and Technology
ISSN: 2576-8484
Vol. 10, No. 1: 102-127, 2026
DOI: 10.55214/2576-8484.v10i1.11532

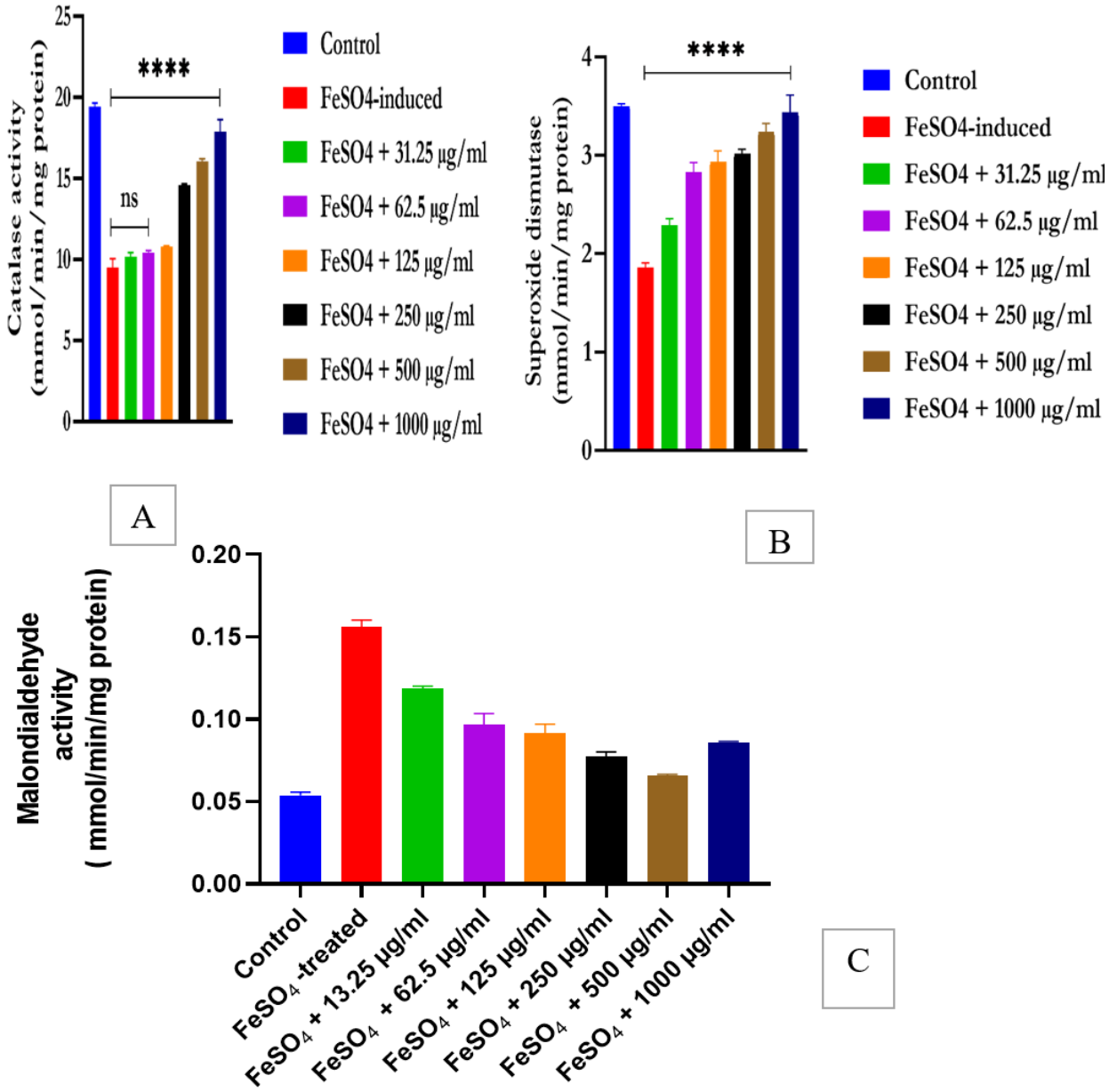

Figure 2.
Ex vivo antioxidant activities of Mondai whitei roots in $FeSO_4^+$-treated liver injury: **(A)** catalase activity, **(B)** superoxide dismutase activity, and **(C)** MDA content (malondialdehyde) levels, with the data shown as the means ± SDs (standard deviations).

3.3. In Vitro Antidiabetic Studies

In vitro studies revealed that *Mondai whitei* extract inhibits α-amylase and α-glucosidase enzymes. Compared with the standard, the extract exhibited substantial inhibitory activity against α-amylase and α-glucosidase (Figures 3 & 4) in a concentration-dependent manner. *Mondai whitei* extract potently inhibited α-amylase and α-glucosidase at every tested concentration, with an IC_{50} of 81.60 ± 0.78 µg/ml. Acarbose had an 82% inhibitory effect on α-glucosidase. *Mondai whitei* extract potently inhibited α-amylase and α-glucosidase, with an IC_{50} of 81.60 ± 0.78 µg/ml. The extract's highest inhibition level

Edelweiss Applied Science and Technology
ISSN: 2576-8484
Vol. 10, No. 1: 102-127, 2026
DOI: 10.55214/2576-8484.v10i1.11532

was approximately 66% for both α-amylase and α-glucosidase, whereas that of acarbose reached approximately 82% for both enzymes.

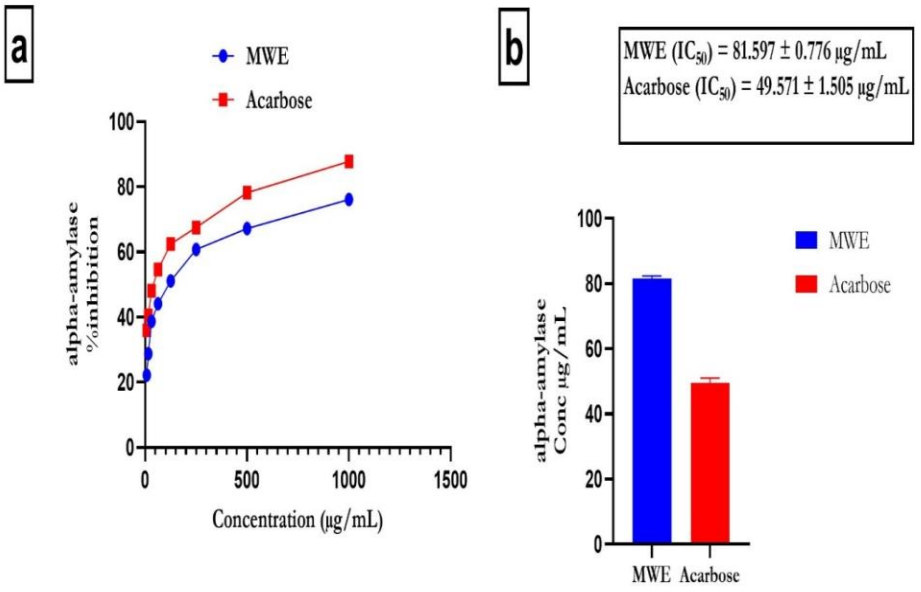

Figure 3.
Inhibition of α-amylase by the ethanolic extract of *Mondai whitei* root is shown, with the data presented as the means ± standard deviations (SDs).

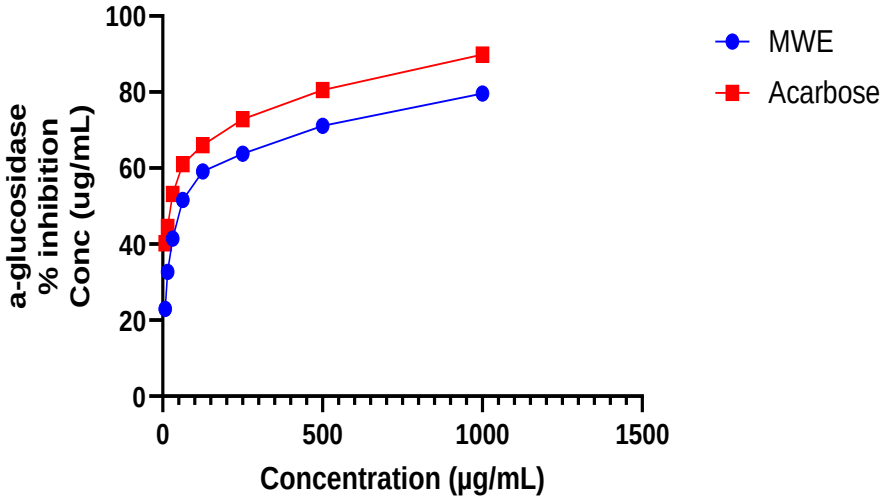

Figure 4.
Inhibition of A-Glucosidase by the Ethanolic Extract of *Mondai Whitei* Root Is Shown, with the Data Presented as The Means ± Standard Deviations (SDs).

Edelweiss Applied Science and Technology
ISSN: 2576-8484
Vol. 10, No. 1: 102-127, 2026
DOI: 10.55214/2576-8484.v10i1.11532

3.4. In Vitro Anti-Inflammatory Studies

Mondai whitei extract stabilized the membrane (IC_{50}= 82.35±2.32 µg/mL). The reference medication, diclofenac, had an IC_{50} of 49.32±0.27 µg/mL (IC_{50} = 89.50%). The ability of *Mondai whitei* extract to suppress protein denaturation increased with increasing concentration. The reference medication diclofenac also decreased protein denaturation (Figure 5a, 5b). *Mondai whitei* extract exhibited notable proteinase inhibitory activity (IC_{50} = 58.72±1.96 µg/mL). However, diclofenac (reference drug) had proteinase inhibitory effects (IC_{50} = 40.42±0.55 µg/mL) (Figure 5c).

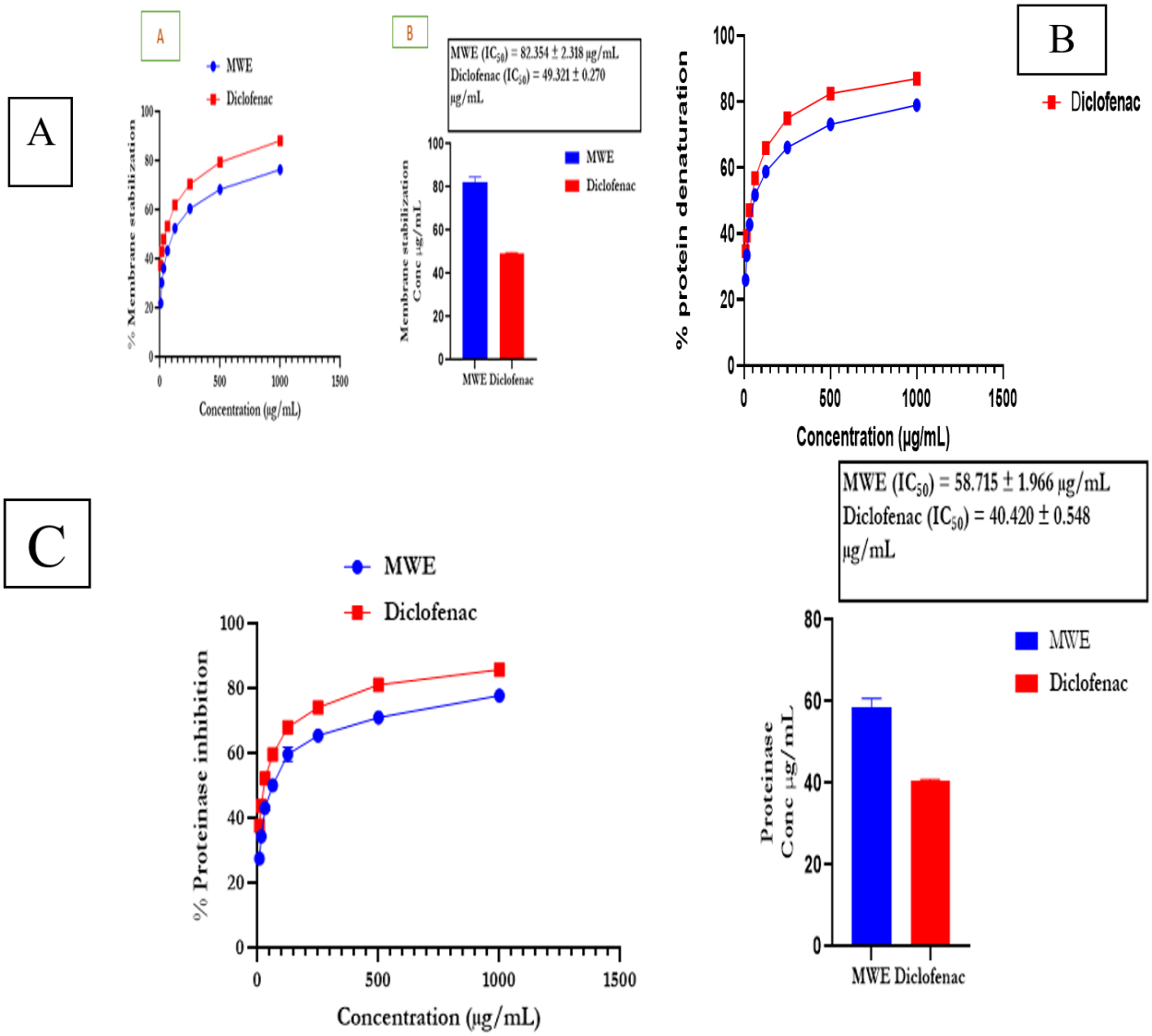

Figure 5.
In vitro inflammatory activities of the ethanolic extracts of Mondai whitei roots: (A) membrane stabilization, (B) protein denaturation inhibition, and (C) proteinase inhibition. The data are presented as the means ± standard deviations (SDs).

3.5. High–Performance Liquid Chromatography (HPLC) Analysis

HPLC was used to identify the phytoconstituents in the *Mondai whitei* extract, which resulted in the identification of 17 phytocompounds, the results of which are included in Table 1. In *Mondai whitei*, the

Edelweiss Applied Science and Technology
ISSN: 2576-8484
Vol. 10, No. 1: 102-127, 2026
DOI: 10.55214/2576-8484.v10i1.11532

two most prevalent compounds were 2-chloro-4-methoxybenzaldehyde (27.948%), vanillin (23.848%), and 5-chloropropacin (12.939%). Dopamine (1.185%), heptacosane (0.997%), and apiole (0.865%) were found in small amounts.

Table 1.
Phytoconstituents of the *Mondai whitei* ethanolic extract detected via HPLC analysis.

S/N	R.T.	Compounds	Molecular Formula	Molecular Weight	Area %	Structure
1	3.700	2-chloro-4-methoxybenz-ald	$C_7H_7ClO_3$	174.58 g/mol	27.948	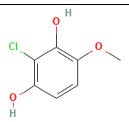
2	5.883	Propacin	$C_{20}H_{18}O_8$	370.359 g/mol	9.573	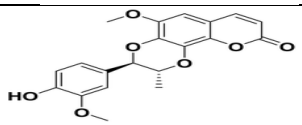
3	7.233	Loliolide	$C_{11}H_{16}O_3$	196.24 g/mol	1.185	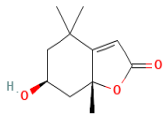
4	7.966	5-chloropropacin	C_3H_7CI	78.541 g/mol	12.939	
5	9.116	Dopamine	$C_6H_{11}NO_2$	153.178 g/mol	1.185	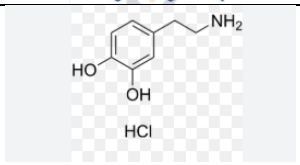
6	10.500	Norepinephrine	$C_8H_{11}NO_3$	169.18 g/mol	1.373	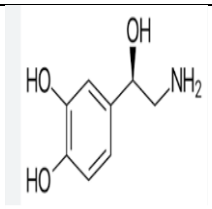
7	11.116	Coumarin	$C_9H_6O_2$	146.143 g/mol	0.771	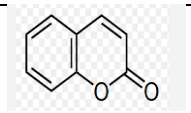
8	11.850	Serotonin	$C_{10}H_{12}N_2O$	176.21 g/mol	1.768	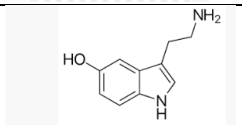

Edelweiss Applied Science and Technology
ISSN: 2576-8484
Vol. 10, No. 1: 102-127, 2026
DOI: 10.55214/2576-8484.v10i1.11532

9	12.816	Apiole	$C_{12}H_{14}O_4$	222.24 g/mol	0.865	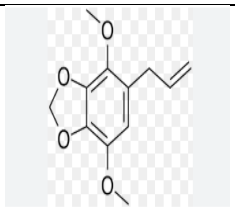
10	13.833	Linalool	$C_{10}H_{18}O$	154.25 g/mol	1.016	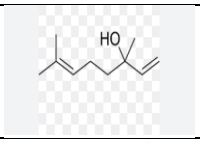
11	15.500	Yohimbine	$C_{21}H_{26}N_2O_3$	354.44 g/mol	12.357	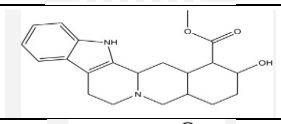
12	17.233	Vanillin	$C_8H_8O_3$	152.15 g/mol	23.848	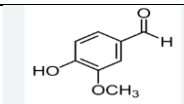
13	19.166	Isovanillin	$C_8H_8O_3$	152.15 g/mol	0.922	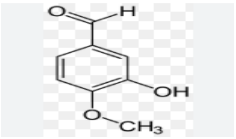
14	20.183	B-ionone	$C_{13}H_{20}O$	192.30 g/mol	1.147	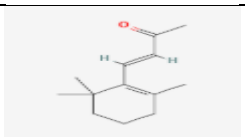
15	21.066	Camphenone	$C_{10}H_{14}O$	152.23 g/mol	1.128	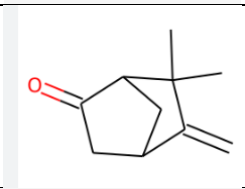
16	21.066	Heptacosane	$C_{27}H_{56}$	380.73 g/mol	0.997	
17	23.083	Fenchol	$C_{10}H_{18}O$	154.25 g/mol	0.809	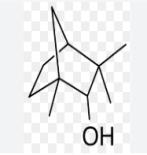

Edelweiss Applied Science and Technology
ISSN: 2576-8484
Vol. 10, No. 1: 102-127, 2026
DOI: 10.55214/2576-8484.v10i1.11532

Table 2.
The binding scores of the selected compounds and reference standards (acarbose and vildagliptin) derived from docking analyses against the three targets.

S/No	Compounds	Binding Scores (Kcal/mol)		
		1B2Y	3TOP	6B1E
	Acarbose	-7.2	-7	-7
	Vildagliptin			-6.9
1	5-Chloropropacin	-9.8	-9.6	-8.1
2	Propacin	-9.5	-8.4	-7.9
3	Yohimbine	-8.8	-9.2	-7.6
4	Loliolide	-6.8	-6	-5.8
5	Beta_Ionone	-6.4	-6.7	-5.8
6	Fenchol	-6.1	-5.7	-5.1
7	Camphenone	-6	-5.6	-4.6
8	Coumarin	-6	-7.1	-5.7
9	Serotonin	-6	-6.8	-5.6
10	Apiole	-5.9	-6.9	-5.6
11	Dopamine	-5.7	-6.4	-5.4
12	Heptacosane	-5.7	-5.5	-4.3
13	Norepinephrine	-5.7	-6.4	-5.4
14	Vanillin	-5.5	-6.1	-5.1
15	2-chloro-4-methoxybenzald	-5.4	-5.8	-4.6
16	Isovanillin	-5.3	-6.1	-5.4
17	Linalool	-5.1	-6.1	-5.4

3.5.1. Binding Affinity of Identified Compounds Against Protein Targets

Table 2 presents the binding scores (in kcal/mol) of the HPLC-identified compounds compared with the reference standards (acarbose for vildagliptin, a known antidiabetic drug, against alpha-amylase). The top-ranked compounds against glucosidase were chloropropacin (-9.6 kcal/mol) and yohimbine (-9.2 kcal/mol). The two top-ranked compounds against DPP IV were 5-chloropropacin (-8.1 kcal/mol) and propacin (-7.9 kcal/mol).

3.6. Interaction of the Top Two Ranked Bioactive Compounds from the Docking Analysis with Protein Targets

The two top-ranked compounds, selected based on binding energy and interaction with the target, were then subjected to interaction analysis. Acarbose was stabilized at the α-amylase binding site via several hydrogen bonds with Leu237, Gly306, His305, His101, and Asp300; alkyl contact with Leu162, Tyr151, and His201; and several van der Waals interactions. 5-Chloropropacin formed hydrogen bonds with Gln63, Pi–Pi stacking with Trp59, and an alkyl contact with His305. Propacin is stabilized mostly by hydrophobic interactions, including pi-cations with His201, pi-anions with Glu233, pi-sigma contacts with Tyr62, and pi-alkyl and alkyl contacts with Tyr151 (Figure 6a). Acarbose was stabilized at the binding site of α-glucosidase via hydrogen bonds with Ly1164 and Trp1369 and several van der Waals interactions. 5-Chloropropacin was also stabilized by hydrogen bonding with Lys1460; Pi–Pi stacking with Trp1369 and Phe1560; pi–pi T-shaped interactions with Tryp1251; and Pi–alkyl and alkyl interactions with Ile1587 and Trp1355. (Figure 6b). Yohimbine interacted via hydrogen bonds with Asp1526; Pi-sigma contacts with Trp1369; pi-pi T-shaped interactions with Phe1559, Trp1355, and Tyr1251; and Pi-alkyl and alkyl interactions with Phe1427, Lys1460, and Phe1560. Vildagliptin was stabilized at the DPPIV binding site via hydrogen bonds with Arg125, Glu205, Glu206, and Val207; pi–alkyl interactions with Tyr666; and numerous van der Waals interactions (Figure 6c).

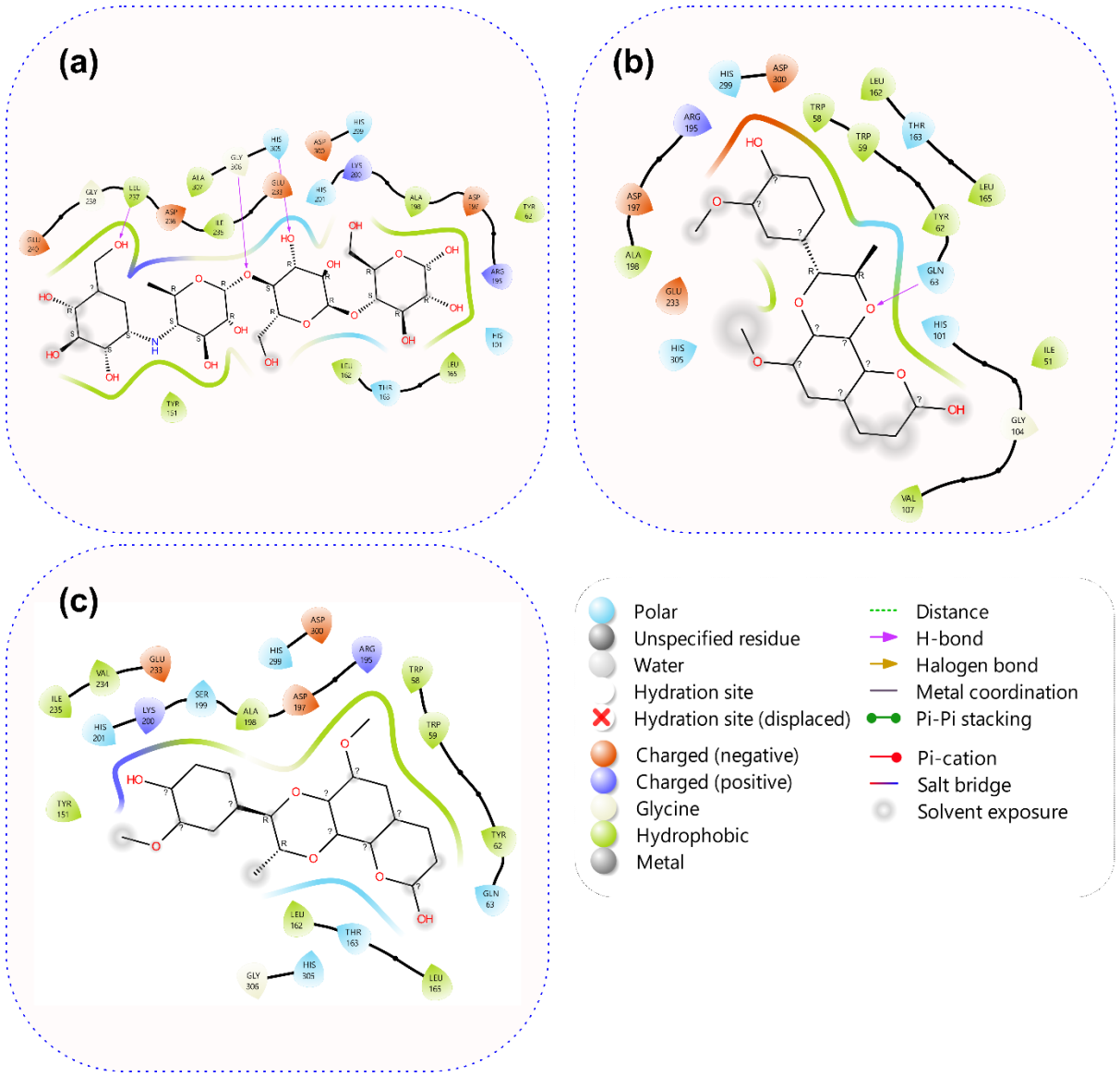

Figure 6(a).
Amino acid interaction plots of the top two compounds and reference compounds (acarbose) from the docking analysis of the binding pocket of human pancreatic α-amylase. (a) acarbose (b) 5-Chloropropacin (c) Propacin

Edelweiss Applied Science and Technology
ISSN: 2576-8484
Vol. 10, No. 1: 102-127, 2026
DOI: 10.55214/2576-8484.v10i1.11532

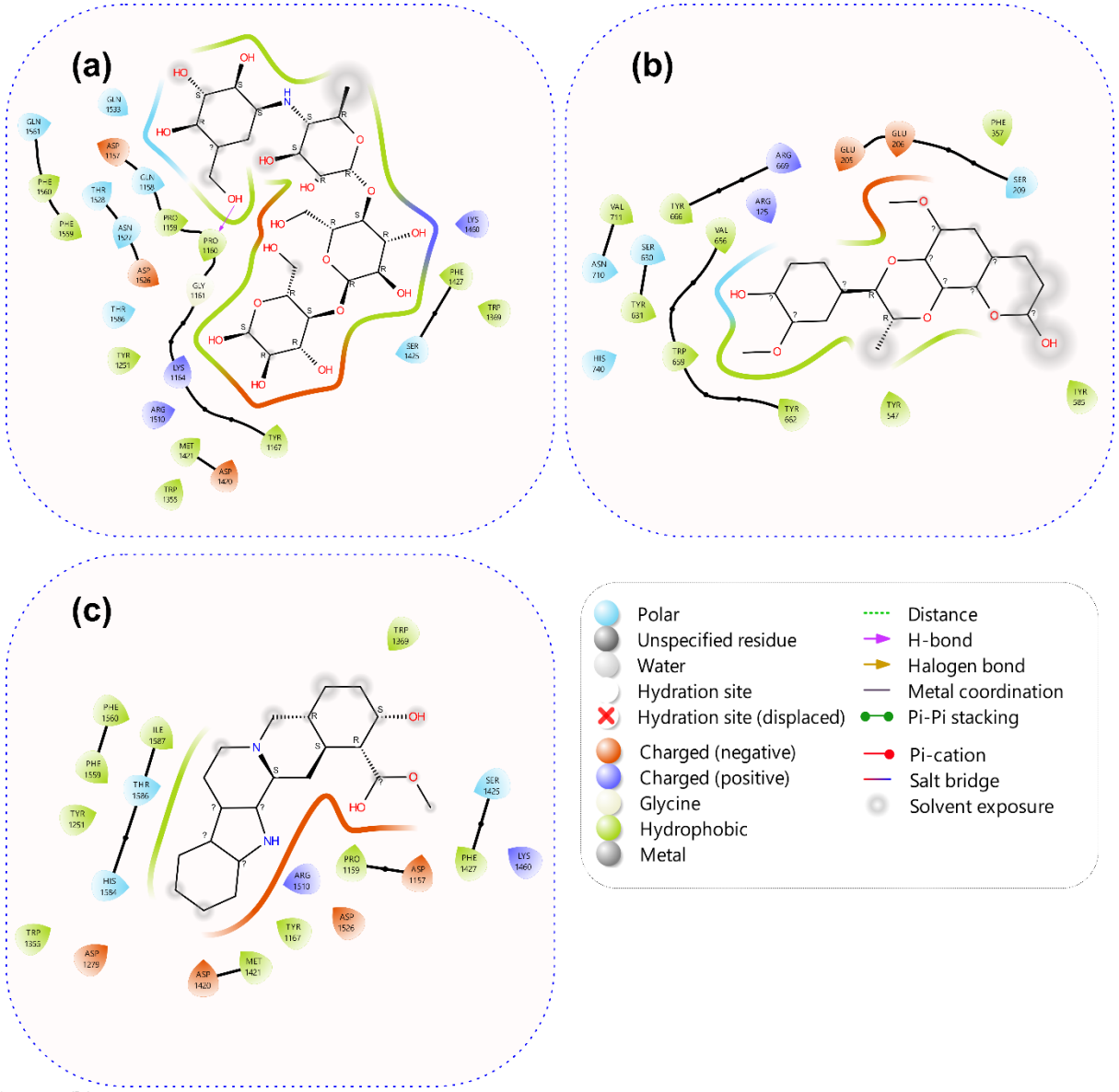

Figure 6(b).
Amino acid interaction plots of the top compounds from docking analysis in the binding pocket of human glucosidase. (a) Acarbose (b) 5-Chloropropacin (c) Yohimbine.

Edelweiss Applied Science and Technology
ISSN: 2576-8484
Vol. 10, No. 1: 102-127, 2026
DOI: 10.55214/2576-8484.v10i1.11532

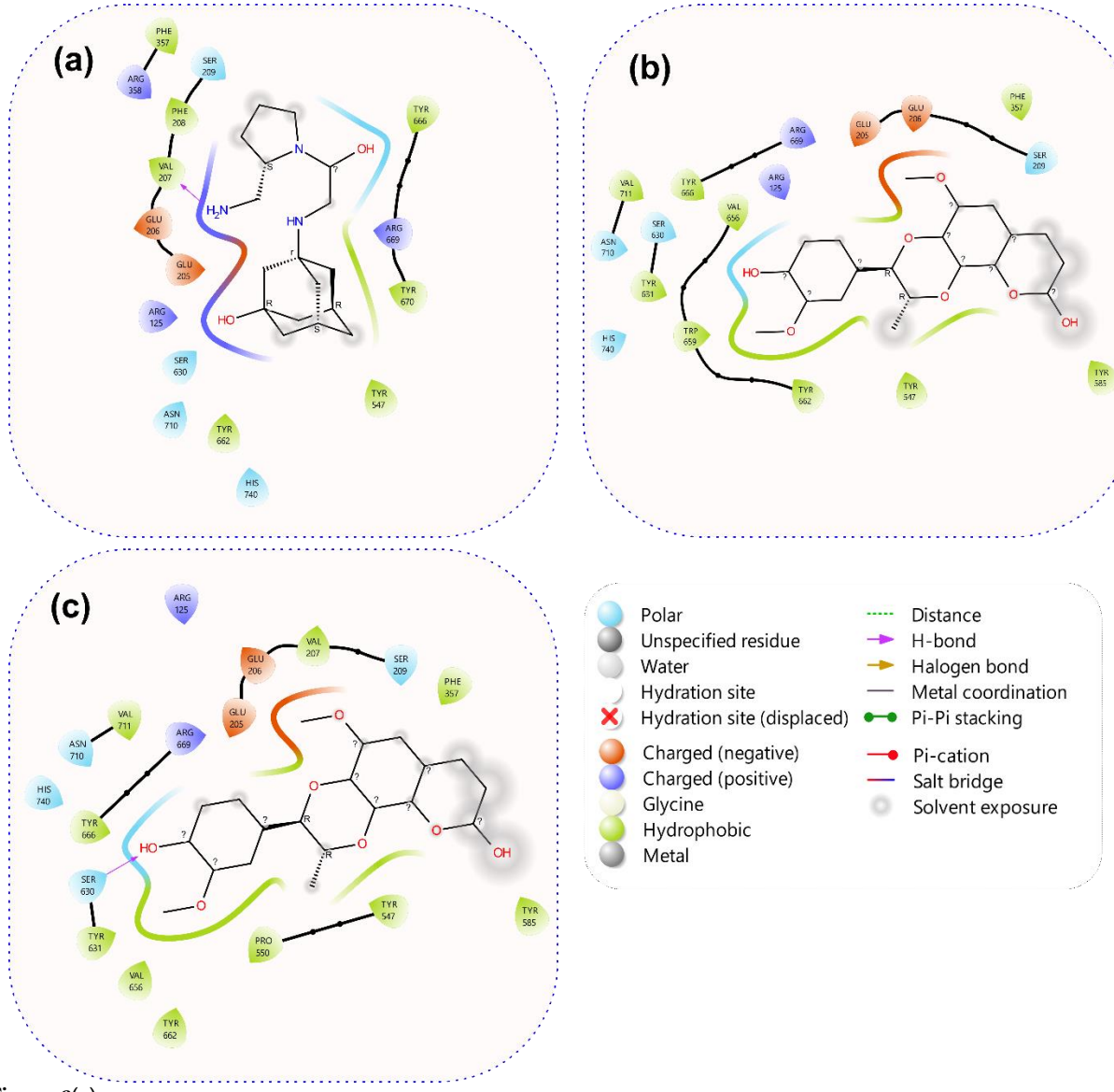

Figure 6(c).
Amino acid interaction plots of the top two compounds from the docking analysis in the binding pocket of DPPIV. (a) Vildagliptin (b) 5-Chloropropacin (c) Propacin

3.7. Thermodynamic Properties of Bound and Unbound Proteins Based on Molecular Dynamics Analysis

All three complexes exhibited very similar and low RMSD values (~1.5 Å), indicating that the protein–ligand complexes were stable throughout the simulation. The 5-chloropropacin complex, which showed the most favorable binding free energy, also remained stable during MD, indicating the reliability of the predicted affinity (Table 3; Figure 7).

Table 3.
Means and standard deviations of the thermodynamic parameters of the two secondary metabolites and the reference standard (acarbose) against the active site of *α-amylase*.

Mean	RRMSD (Å)	RMSF (Å)	RoG (Å)	SASA (Å)	H - Bond
1B2Y_Propacin	1.48 ± 0.20	0.98 ± 0.59	23.18 ± 0.06	17530.6 ± 481.48	258.33 ± 10.61
1B2Y_5-Chloropropacin	1.49 ± 0.19	1.02 ± 0.61	23.16 ± 0.07	17226.5 ± 450.26	263.51 ± 11.09
1B2Y_Acarbose	1.50 ± 0.23	1.02 ± 0.74	23.20 ± 0.11	17750.9 ± 623.31	264.64 ± 10.70

All three complexes have similar mean RMSF values, ranging from 0.98 to 1.02 Å, suggesting comparable overall protein flexibility in the presence of the three ligands (Figure 8).

A higher RoG implies slight expansion or flexibility in the protein. All the RoG values are very close (approximately 23.16–23.20 Å). 1B2Y_5-Chloropropacin (23.16 ± 0.07 Å) presented the lowest mean RoG, implying that it may induce slightly more compact folding than the other compounds do (Figure 8).

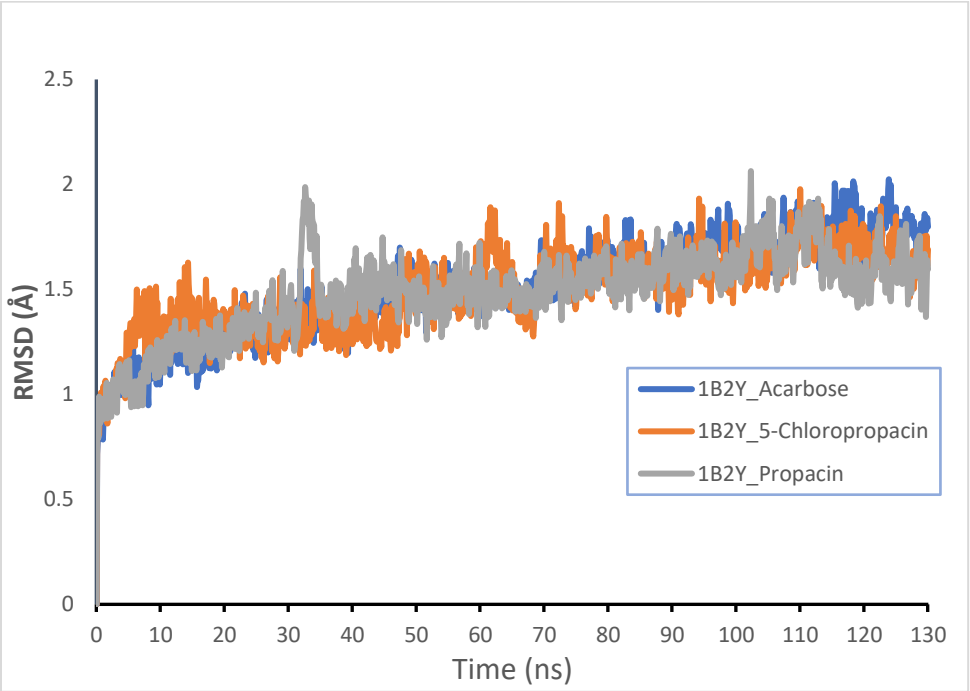

Figure 7.
Backbone-root mean square deviation (RMSD) plots of MD simulations of reference compounds (acarbose) and the top two phytochemicals from the docking analysis against human pancreatic α-amylase.

Edelweiss Applied Science and Technology
ISSN: 2576-8484
Vol. 10, No. 1: 102-127, 2026
DOI: 10.55214/2576-8484.v10i1.11532

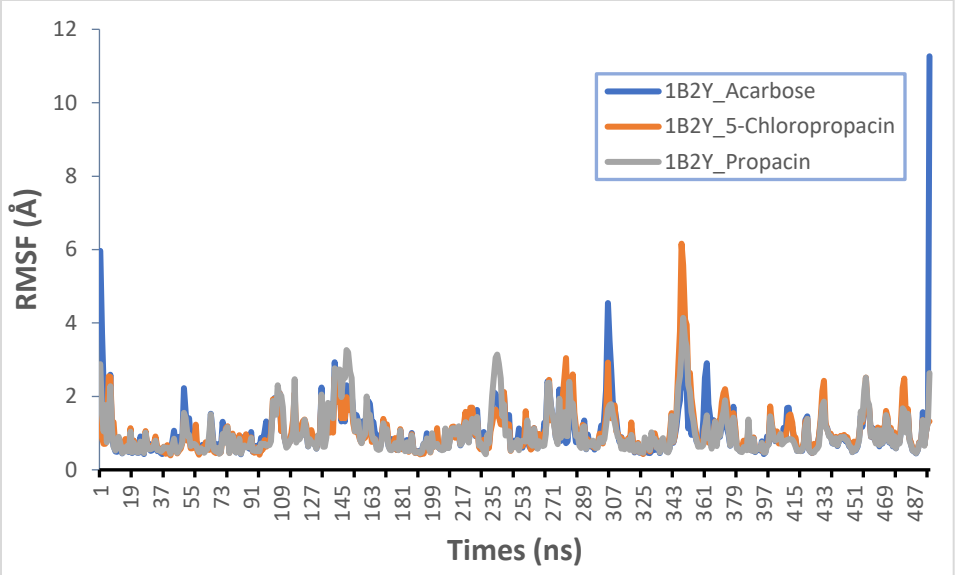

Figure 8.
Per-residue root mean square fluctuation (RMSF) plots of MD simulations of reference compounds (acarbose) and the top two phytochemicals from the docking analysis against human pancreatic α-amylase.

1B2Y_5-chloropropacin (17,226.5 ± 450.26 Å²) presented the lowest mean SASA among the three complexes was observed in 1B2Y_Propacin, with a SASA of 17,530.6 ± 481.48 Å², which was slightly greater than that of 5-chloropropacin. The reference standard system, 1B2Y_Acarbose, exhibited the highest SASA at 17,750.9 ± 623.31 Å², along with the largest standard deviation, indicating greater exposure to solvent. This may reflect more surface rearrangement or flexibility (Figure 10). A greater number of hydrogen bonds generally implies stronger and more stable binding. *2-Benzoyl and methyl esters* form the largest average number of hydrogen bonds, totaling 272.7, suggesting strong and stable interactions with the 1B2Y protein. Acarbose forms 267.4 hydrogen bonds, slightly fewer than *2-benzoyl- and methyl esters*. The benzeneamine and 4-methyl-3-nitro groups form the fewest hydrogen bonds, with a total of 262.1 (Figure 11).

Edelweiss Applied Science and Technology
ISSN: 2576-8484
Vol. 10, No. 1: 102-127, 2026
DOI: 10.55214/2576-8484.v10i1.11532

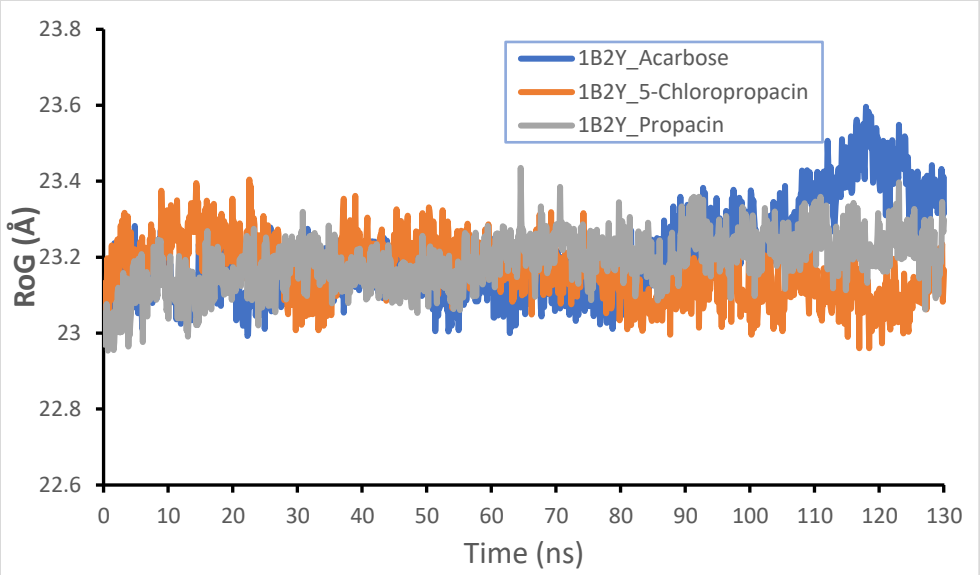

Figure 9.
Radius of gyration (RoG) plots of MD simulations of reference compounds (acarbose) and the top two phytochemicals from the docking analysis against human pancreatic α-amylase.

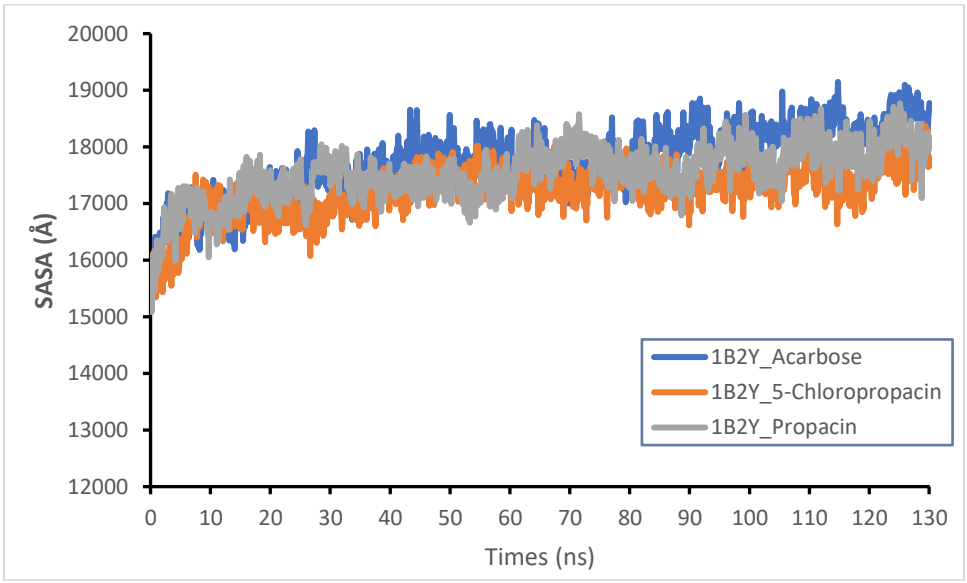

Figure 10.
Solvent Accessible Surface Area (SASA) plots of molecular docking (MD) simulations of reference compounds (Acarbose) and the top two phytochemicals from docking analysis against human pancreatic alpha-amylase.

Edelweiss Applied Science and Technology
ISSN: 2576-8484
Vol. 10, No. 1: 102-127, 2026
DOI: 10.55214/2576-8484.v10i1.11532

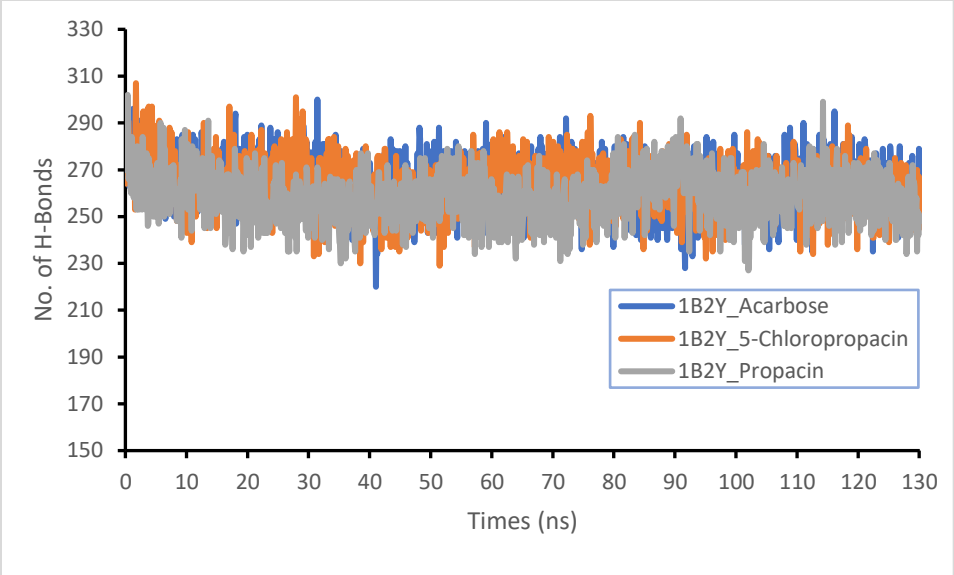

Figure 11.
Variations in the number of hydrogen-bond plots of molecular docking simulations of reference compounds (acarbose) and the top two phytochemicals from the docking analysis against human pancreatic α-amylase.

3.8. Molecular Mechanics Generalized Born Surface Area (MMGBSA) Analysis of the Top-Docked Compounds

The 1B2Y_5-chloropropacin complex exhibited the most favorable (lowest) ΔTOTAL energy of -24.40 ± 3.28 kcal/mol, suggesting strong binding affinity. Strong van der Waals (−36.82 kcal/mol) and electrostatic interactions (−20.77 ± 3.10 kcal/mol) dominate, although the polar solvation energy (ΔEGB = +30.35 ± 4.04 kcal/mol) partially offsets this. The highly negative ΔGGAS (−50.28 ± 5.85 kcal/mol) confirms strong gas-phase interactions. Among the three systems, the 1B2Y_propacin system has a moderately favorable total binding energy (−18.26 ± 3.88 kcal/mol). Greater van der Waals interactions (−30.25 ± 4.06 kcal/mol) and low electrostatics (−9.96 ± 8.10 kcal/mol) were the major drivers of the interactions. The 1B2Y_acarbose system shows the least binding (−6.73 ± 8.25 kcal/mol), with a large electrostatic contribution (−50.44 kcal/mol) but high variability (± 8.25) (Table 4).

Table 4.
Provides detailed results of the various energy components that make up the total BFE (Δ_{TOTAL}).

Systems	$\Delta_{VDWAALS}$	Δ_{EEL}	ΔE_{GB}	ΔE_{SUR}	ΔG_{GAS}	ΔG_{SOLV}	Δ_{TOTAL}
1B2Y_Propacin	-30.25 ± 4.06	-9.96 ± 8.10	26.12 ± 6.55	-4.17 ± 0.53	-40.21± 8.67	21.95 ± 6.31	-18.26 ± 3.88
1B2Y_5-Chloropropacin	−20.77± 3.10	-12.44 ± 4.89	30.35 ± 4.04	-4.46 ± 0.36	-50.28 ± 5.85	25.88 ± 3.93	-24.40 ± 3.28
1B2Y_Acarbose	−21.06 ± 8.49	−50.44 ± 27.31	68.18 ± 28.85	−3.41 ± 1.22	−71.50 ± 31.52	64.77± 28.04	−6.73 ± 8.25

3.9. Pharmacokinetic and ADMET Properties of the Top-Ranked Compounds

ADMET and the predicted pharmacokinetic and chemical characteristics are presented in Table 3. 5-Chloropropacin is slightly heavier due to the added chlorine atom. Both values are within Lipinski's acceptable range (<500 g/mol). Both compounds presented equal flexibility, which is favorable for oral bioavailability. 5-Chloropropacin has a relatively high TPSA, which may reduce passive membrane permeability slightly, but both values are within the acceptable range for oral drugs (<140 Å²). Both are moderately lipophilic, with 5-chloropropacin being slightly more hydrophobic, possibly aiding in membrane permeability. Both compounds were predicted to be well absorbed in the intestine, with a

Edelweiss Applied Science and Technology
ISSN: 2576-8484
Vol. 10, No. 1: 102-127, 2026
DOI: 10.55214/2576-8484.v10i1.11532

slightly greater amount of 5-chloropropacin. Both compounds showed modest synthetic accessibility scores of less than 5.

Table 5.
Predicted Pharmacokinetics and ADMET Properties of the Top Two Compounds.

	5-Chloropropacin	**Propacin**
Molecular weight (g/mol)	404.80	370.35
Num. heavy atoms	28	27
Num. arom. Heavy atoms	16	16
Num. rotatable bonds	3	3
Num. H-bond acceptors	7	7
Hydrogen bond donor	1	1
Molar Refractivity		97.66
TPSA Å²	102.16	87.36
MLogP	1.94	1.44
Drug-likeness		
Lipinski	Yes	Yes
Veber	Yes	Yes
Ghose	Yes	Yes
Egan	Yes	Yes
Absorption (Probability)		
HIA	HIA+ (0.649)	HIA+ (0.628)
P-Glycoprotein substrate	Neg. (0.044)	Neg. (0.041)
Distribution (Probability)		
PPB% Metabolism (Probability)	81.714	82.213
CYP450 1A2 Inhibitor	Neg. (0.412)	Neg. (0.444)
CYP450 1A2 Substrate	Pos. (0.509)	Pos. (0.546)
CYP450 3A4 Inhibitor	Neg. (0.253)	Neg. (0.451)
CYP450 3A4 Substrate	Neg (0.744)	Neg. (0.498)
Elimination		
$T_{1/2}$ (Half Life Time)	1.687 h	1.936 h
CL (Clearance Rate) mL/min/kg	1.465	1.715
Toxicity		
hERG Blockers	Pos. (0.532)	Neg. (0.712)
SkinSen (Skin sensitization)	Neg. (0.284)	Neg. (0.098)
AMES	Neg. (0.286)	Neg. (0.418)
Carcinogen	Neg. (0.8698)	Neg. (0.133)
Synthetic accessibility	4.48	4.43

4. Discussion

The use of plant extracts is becoming more popular in the fight against a variety of ailments and diseases because of the numerous phytochemicals they contain, which increase the number of free radicals in the body's systems [38]. When unpaired electrons in the system interact with proteins and enzymes through a process known as glycation, they result in oxidative stress [20]. Thus, the purpose of this study was to evaluate the anti-inflammatory, antidiabetic, antioxidant, and phytochemical properties of *M. whitei* roots. To determine the most effective form of the plant for controlling inflammation, oxidative stress, and diabetes, this evaluation was conducted via *in vitro*, *ex vivo*, and *in silico* approaches. Numerous bioactive substances, including tannins, alkaloids, phenols, flavonoids, steroids, and glycosides, are considered secondary metabolites and are primarily responsible for the biological effects of medicinal plants [39]. In traditional medical practices, these compounds work either alone or in combination to reduce the severity of a number of diseases. Additionally, they contain an abundance of lead compounds that can be utilized to create various medications for a variety of illnesses

Edelweiss Applied Science and Technology
ISSN: 2576-8484
Vol. 10, No. 1: 102-127, 2026
DOI: 10.55214/2576-8484.v10i1.11532

[40, 41]. The extract of *Mondai whitei* was examined for possible phytochemicals. The *in vitro* analysis findings indicate that DPPH-scavenging radicals are widely known for their exceptional scavenging abilities and that the extract has a relatively high degree of DPPH quenching potential. These findings suggest that the extract from *Mondai whitei* includes potent antioxidants that can eliminate free radicals from the body. The ability of the extract to fight ROS and decrease the chance of oxidative stress was further demonstrated by FRAP analysis. Given that oxidative stress adversely affects glucose metabolism, the CAT and SOD levels in the treated groups increased, whereas lipid peroxidation activity decreased as the concentration of the extract increased, suggesting that the extract has positive effects on hepatic tissue [42].

Alpha-amylase and alpha-glucosidase are the two primary enzymes involved in carbohydrate metabolism, which are considered novel approaches for regulating postprandial hyperglycemia associated with diabetes mellitus (DM) [43, 44]. Currently, the first line of treatment is pharmacological management using oral antidiabetic medications (acarbose, metformin, etc.), which function mainly as inhibitors of α-amylase and α-glucosidase enzymes in carbohydrate metabolism. Unfortunately, these medications are associated with a number of adverse effects, such as diarrhea, bloating, flatulence, and other health problems [45]. Accordingly, postprandial hyperglycemia linked to diabetes mellitus can be effectively treated and managed with inhibitors of these enzymes derived from medicinal herbs [46, 47]. *Mondai whitei* extract exhibited moderate levels of inhibitory activity against α-amylase and α-glucosidase. The alpha-amylase and alpha-glucosidase inhibitory effects of the *M. whitei* extract were concentration-dependent, with greater inhibitory effects observed at 1500 µg/ml.

Inflammation is a complex biological reaction that depends on a number of indicators, one of which is protein denaturation in tissues. To assess the *in vitro* anti-inflammatory potency of the extract, the inhibitory effect of *Mondai whitei* extract on inflammatory markers such as membrane stabilization, protein denaturation, and proteinase activity was examined. The results indicated that the extract significantly decreased protein denaturation, and since diclofenac has a slightly greater protective effect, the *Mondai whitei* extract might be a good choice for anti-inflammatory drugs.

The ability of *M. whitei* extract to inhibit proteinases, which are frequently implicated in the inflammatory process, was investigated to determine its possible anti-inflammatory effects. These results show that the extract can inhibit proteinase enzymes but not as effectively as diclofenac. The ability to stabilize HRBC membranes is a sign of anti-inflammatory action because lysosomes may produce certain chemicals during inflammation, which might lead to complications. Lysosomal membranes can be protected from harm via a mechanism called membrane stabilization. *Mondai whitei* showed promise in stabilizing lysosomal membranes in this investigation by protecting HRBC membranes from heat-induced damage. These results suggest that the ability of the HRBC membrane to stabilize *M. whitei* extract is related to its anti-inflammatory properties.

Through HPLC analysis, 17 compounds were identified as bioactive substances that may be involved in the actions outlined above of the M. whitei extract. The selection of the three compounds with the highest binding affinities against each target protein was based on their docking scores (binding affinities), where more negative values indicate stronger and more favorable binding interactions with the protein target. 5-Chloropropacin (-9.8 kcal/mol) and propacin (-9.5 kcal/mol) were the top-ranked compounds against alpha-amylase. These compounds exhibited the lowest (most negative) docking scores among all the tested ligands, indicating strong binding potential to the 1B2Y target, likely due to optimal molecular fit and interaction with active site residues. The top-ranked compounds against glucosidase were chloropropacin (-9.6 kcal/mol) and yohimbine (-9.2 kcal/mol). These compounds presented the strongest binding affinities toward 3TOP. These values suggest favorable interaction energies, possibly from key hydrogen bonding and hydrophobic interactions within the receptor pocket. The two top-ranked compounds against DPPIV were 5-chloropropacin (-8.1 kcal/mol) and propacin (-7.9 kcal/mol). Despite generally lower binding scores across the board for 6B1E than for the other targets, 5-chloropropacin and propacin again ranked highest, confirming their

Edelweiss Applied Science and Technology
ISSN: 2576-8484
Vol. 10, No. 1: 102-127, 2026
DOI: 10.55214/2576-8484.v10i1.11532

broad-spectrum binding effectiveness. At the atomic level, molecular dynamics (MD) simulation is a powerful computational tool that provides comprehensive insights into the dynamic behavior of biomolecules and their interactions with potential therapeutic options. Through continuous tracking of atomic movements over time, MD simulations allow researchers to observe how a drug molecule binds to its target, how stable that binding is, and what conformational changes may occur in both the ligand and the biomolecule during the interaction [48]. The RMSD (root mean square deviation) measures the average deviation of the protein–ligand complex structure from its initial configuration over the simulation. Lower RMSD values suggest greater structural stability [49]. The root mean square fluctuation (RMSF) quantifies the average displacement of each residue from its mean position over the simulation. A lower RMSF indicates less fluctuation, suggesting greater rigidity and potential stability of the protein structure. Conversely, a higher RMSF suggests more flexible or disordered regions, which may affect binding stability [49]. The addition of a chlorine atom could induce local structural perturbations or weaker binding interactions, leading to a small increase in overall flexibility. RoG measures the distribution of atoms around the protein's center of mass. The protein structure is more compact when the RoG is lower, which is often associated with better structural stability [50]. A higher RoG implies slight expansion or flexibility in the protein. All the RoG values are very close (approximately 23.16–23.20 Å). This finding shows that none of the ligands cause major structural expansion or compaction of the protein. 1B2Y_5-Chloropropacin (23.16 ± 0.07 Å) presented the lowest mean RoG, implying that it may induce slightly more compact folding than the other compounds. The 1B2Y_propacin (23.18 ± 0.06 Å) system presented very close compactness to that of 5-chloropropacin, although it presented a slightly greater mean and slightly lower variability, suggesting a consistently stable structure. The acarbose-bound system (23.20 ± 0.11 Å) presented the highest RoG and largest standard deviation, indicating marginally looser packing and greater fluctuation in protein conformation. The solvent-accessible surface area (SASA) is another key parameter that reflects the surface area of a biomolecule exposed to the solvent. It provides insights into the extent of ligand binding and the degree of protein folding or unfolding [51]. In general, lower SASA values typically indicate a more compact structure with less surface area exposed to the solvent. Higher SASA values may suggest increased surface exposure, possibly due to conformational changes or a more open protein structure. 1B2Y_5-chloropropacin (17,226.5 ± 450.26 Å²) exhibited the lowest mean SASA among the three complexes. These findings imply that this ligand induces the most compact or solvent-shielded conformation of the protein. The SASA of 1B2Y_Propacin (17,530.6 ± 481.48 Å²) was slightly higher than that of 5-chloropropacin. Nonetheless, it maintains a relatively compact structure but is marginally more exposed than its chlorinated analog. The reference standard system (1B2Y_Acarbose (17,750.9 ± 623.31 Å²)) showed the highest SASA and the largest standard deviation, indicating greater exposure to solvent, which may reflect more surface rearrangement or flexibility. This aligns with higher RoG and RMSF variability.

The two top secondary metabolites have lower SASA values (~16,670–16,695 Å²), suggesting that they help maintain or induce a more compact and less solvent-exposed protein conformation. 1B2Y_acarbose exhibited a significantly greater SASA (17,231.8 Å²), indicating that binding with acarbose may result in a more open or flexible structure, increasing the surface area exposed to the solvent. The lower SASA for the complexes with the two top secondary metabolites supports earlier RMSD, RMSF, and RoG findings that these ligands contribute to greater structural compactness and stability.

Hydrogen bonds (H-bonds) are key contributors to the stability and specificity of ligand–protein interactions. A large number of hydrogen bonds generally implies strong and very stable binding. The consistency (low standard deviation) reflects stable interactions throughout the simulation. Additionally, the top two compounds identified by docking analysis were evaluated for their synthetic accessibility, drug-likeness, ADME profiles, toxicity risks, and in silico pharmacokinetic properties to minimize the likelihood of costly failures commonly encountered in the later phases of drug development [52]. A topological polar surface area (TPSA) of less than 140 Å² has been linked with

Edelweiss Applied Science and Technology
ISSN: 2576-8484
Vol. 10, No. 1: 102-127, 2026
DOI: 10.55214/2576-8484.v10i1.11532

good oral absorption and cell membrane permeability [16]. Both compounds passed at least every drug-likeness filter (Lipinski, Veber, Ghose, and Egan), supporting their potential as orally active drugs [53-55]. These compounds exhibit favorable pharmacokinetic properties, such as an appropriate molecular weight and polar surface area, as well as balanced lipophilicity, hydrogen bonding ability, and molecular flexibility, making them compelling subjects for additional research [56].

Both compounds showed high intestinal absorption, indicating that the human gut is likely to absorb the chemical [57]. Both compounds are unlikely to be effluxed by P-gp, which is favorable for bioavailability. Both compounds are unlikely to inhibit CYP1A2, which may reduce the risk of drug–drug interactions but are substrates for CYP1A2, indicating the possibility of their metabolism by CYP3A4. Both have short half-lives; the half-life of propacin is slightly longer, possibly due to lower clearance. 5-Chloropropacin may block hERG channels, increasing the degree of cardiotoxicity. Propacin is safer in this regard. Both compounds are safe in terms of their carcinogenicity and mutagenicity, which makes them promising candidates for further research [58]. Both compounds presented moderate synthetic accessibility scores of less than 5, making them suitable candidates for further development as orally bioavailable drugs [49].

Binding free energy (BFE) calculations, particularly those derived from molecular dynamics (MD) trajectories, play a vital role in validating molecular docking results. They provide a more accurate prediction of the strength and stability of drug–target interactions by incorporating dynamic conformational changes and explicit solvent effects. This allows for more reliable identification and prioritization of promising lead compounds [59].

5. Conclusion

This study provides preliminary compelling evidence that the root extract of *Mondia whitei* has remarkable anti-inflammatory, antidiabetic, and antioxidant properties. These findings are supported by a combination of computational modeling techniques and experimental validation, offering a robust framework for understanding the medicinal potential of plants.

Institutional Review Board Statement:

All the experimental protocols were conducted according to the guidelines for the care and use of experimental animals of Bowen University, Iwo, Osun State, Nigeria. Ethical approval was sought from the University of Ibadan Ethical Committee (UI-ACUREC/M/0051).

Transparency:

The authors confirm that the manuscript is an honest, accurate, and transparent account of the study; that no vital features of the study have been omitted; and that any discrepancies from the study as planned have been explained. This study followed all ethical practices during writing.

Acknowledgments:

Dr. Oluwafemi Ojo has been co-funded by the European Union's Horizon Europe Framework Programme for Research and Innovation 2021–2027 under the Marie Sklodowska-Curie action grant agreement No. 101126611.

References

[1] M. M. I. Abdalla, "Insulin resistance as the molecular link between diabetes and Alzheimer's disease," *World Journal of Diabetes*, vol. 15, no. 7, pp. 1430-1447, 2024. https://doi.org/10.4239/wjd.v15.i7.1430

[2] A. Kapoor, "Probrain mindset for perfect health span and prevention of Alzheimer's Dementia." Bloomington, IN: Xlibris Corporation, 2024.

[3] International Diabetes Federation, *Global burden of diabetes. In Diabetes atlas*, 5th ed. Brussels, Belgium: International Diabetes Federation, 2011.

[4] O.-O. P. Akpoveso, E. E. Ubah, and G. Obasanmi, "Antioxidant phytochemicals as potential therapy for diabetic complications," *Antioxidants*, vol. 12, no. 1, p. 123, 2023.

[5] S. Kumar *et al.*, "The interplay of oxidative stress and ROS scavenging: Antioxidants as a therapeutic potential in sepsis," *Vaccines*, vol. 10, no. 10, p. 1575, 2022. https://doi.org/10.3390/vaccines10101575

[6] M. Wronka, J. Krzemińska, E. Młynarska, J. Rysz, and B. Franczyk, "The influence of lifestyle and treatment on oxidative stress and inflammation in diabetes," *International Journal of Molecular Sciences*, vol. 23, no. 24, p. 15743, 2022.

[7] J. M. Jaffri, "Reactive oxygen species and antioxidant system in selected skin disorders," *The Malaysian Journal of Medical Sciences: MJMS*, vol. 30, no. 1, p. 7, 2023.

[8] N. K. Bhol *et al.*, "The interplay between cytokines, inflammation, and antioxidants: mechanistic insights and therapeutic potentials of various antioxidants and anti-cytokine compounds," *Biomedicine & Pharmacotherapy*, vol. 178, p. 117177, 2024. https://doi.org/10.1016/j.biopha.2024.117177

[9] S. M. Firdous and S. Pal, "Role of inflammatory and Growth factors in diabetes mellitus," *Palestinian Medical and Pharmaceutical Journal*, vol. 9, no. 2, pp. 193-208, 2023.

[10] J. Watral *et al.*, "Comprehensive proteomics of monocytes indicates oxidative imbalance functionally related to inflammatory response in chronic kidney disease-related atherosclerosis," *Frontiers in Molecular Biosciences*, vol. 11, p. 1229648, 2024.

[11] C. A. Thorne, A. C. Grey, J. C. Lim, and P. J. Donaldson, "The synergistic effects of polyol pathway-induced oxidative and osmotic stress in the aetiology of diabetic cataracts," *International Journal of Molecular Sciences*, vol. 25, no. 16, p. 9042, 2024. https://doi.org/10.3390/ijms25169042

[12] S. Alfei, G. C. Schito, A. M. Schito, and G. Zuccari, "Reactive oxygen species (ROS)-mediated antibacterial oxidative therapies: Available methods to generate ROS and a novel option proposal," *International Journal of Molecular Sciences*, vol. 25, no. 13, p. 7182, 2024.

[13] D. Lian, M.-M. Chen, H. Wu, S. Deng, and X. Hu, "The role of oxidative stress in skeletal muscle myogenesis and muscle disease," *Antioxidants*, vol. 11, no. 4, p. 755, 2022.

[14] J. Li, Z. Zhang, H. Bo, and Y. Zhang, "Exercise couples mitochondrial function with skeletal muscle fiber type via ROS-mediated epigenetic modification," *Free Radical Biology and Medicine*, vol. 213, pp. 409-425, 2024. https://doi.org/10.1016/j.freeradbiomed.2024.01.036

[15] H. A. Hassan, H. S. Ahmed, and D. F. Hassan, "Free radicals and oxidative stress: Mechanisms and therapeutic targets," *Human Antibodies*, vol. 32, no. 4, pp. 151-167, 2024.

[16] M. Schrader, I. Castro, H. D. Fahimi, and M. Islinger, *Peroxisome morphology in pathologies. In Molecular machines involved in peroxisome biogenesis and maintenance*. Vienna: Springer Vienna, 2014.

[17] S. K. Ramaiah, *Mechanisms of liver injury and tissue repair in thioacetamide hepatotoxicity following diet restriction*. Unpublished Master's Thesis. Northeast Louisiana University, 1999.

[18] Z. Bi *et al.*, "The generation and transformation mechanisms of reactive oxygen species in the environment and their implications for pollution control processes: A review," *Environmental Research*, vol. 260, p. 119592, 2024.

[19] A. B. Ojo *et al.*, "Syzygium aromaticum (L.) Merr. & LM Perry mitigates iron-mediated oxidative brain injury via in vitro, ex vivo, and in silico approaches," *Journal of Molecular Structure*, vol. 1268, p. 133675, 2022. https://doi.org/10.1016/j.molstruc.2022.133675

[20] S. Ahmad *et al.*, "Secondary metabolite profiling, antioxidant, antidiabetic and neuroprotective activity of cestrum nocturnum (night scented-jasmine): Use of in vitro and in silico approach in determining the potential bioactive compound," *Plants*, vol. 12, no. 6, p. 1206, 2023. https://doi.org/10.3390/plants12061206

[21] B. O. Ajiboye, B. E. Oyinloye, P. E. Agboinghale, and O. A. Ojo, "Cnidoscolus aconitifolius (Mill.) IM Johnst leaf extract prevents oxidative hepatic injury and improves muscle glucose uptake ex vivo," *Journal of Food Biochemistry*, vol. 43, no. 12, p. e13065, 2019.

[22] H. D. McIntyre, P. Catalano, C. Zhang, G. Desoye, E. R. Mathiesen, and P. Damm, "Gestational diabetes mellitus," *Nature Reviews Disease Primers*, vol. 5, no. 1, p. 47, 2019.

[23] I. A. Hogan *et al.*, "Attenuation of hyperglycemia-associated dyslipidemic, oxidative, cognitive, and inflammatory crises via modulation of neuronal ChEs/NF-κB/COX-2/NOx, and hepatorenal functional deficits by the Tridax procumbens extract," *Biomedicine & Pharmacotherapy*, vol. 158, p. 114114, 2023. https://doi.org/10.1016/j.biopha.2022.114114

[24] M. Bouslamti *et al.*, "Phenolic profile, inhibition of α-amylase and α-glucosidase enzymes, and antioxidant properties of Solanum elaeagnifolium Cav.(Solanaceae): In vitro and in silico investigations," *Processes*, vol. 11, no. 5, p. 1384, 2023. https://doi.org/10.3390/pr11051384

[25] N. M. O'Boyle, M. Banck, C. A. James, C. Morley, T. Vandermeersch, and G. R. Hutchison, "Open Babel: An open chemical toolbox," *Journal of Cheminformatics*, vol. 3, no. 1, p. 33, 2011.

[26] V. NAHOUM *et al.*, "Crystal structures of human pancreatic α-amylase in complex with carbohydrate and proteinaceous inhibitors," *Biochemical Journal*, vol. 346, no. 1, pp. 201-208, 2000.
[27] G. M. Morris *et al.*, "AutoDock4 and AutoDockTools4: Automated docking with selective receptor flexibility," *Journal of Computational Chemistry*, vol. 30, no. 16, pp. 2785-2791, 2009.
[28] O. Trott and A. J. Olson, "AutoDock Vina: improving the speed and accuracy of docking with a new scoring function, efficient optimization, and multithreading," *Journal of Computational Chemistry*, vol. 31, no. 2, pp. 455-461, 2010. https://doi.org/10.1002/jcc.21334
[29] C. Oostenbrink, A. Villa, A. E. Mark, and W. F. Van Gunsteren, "A biomolecular force field based on the free enthalpy of hydration and solvation: the GROMOS force-field parameter sets 53A5 and 53A6," *Journal of Computational Chemistry*, vol. 25, no. 13, pp. 1656-1676, 2004.
[30] M. J. Abraham *et al.*, "GROMACS: High performance molecular simulations through multi-level parallelism from laptops to supercomputers," *SoftwareX*, vol. 1, pp. 19-25, 2015.
[31] B. R. Brooks *et al.*, "CHARMM: the biomolecular simulation program," *Journal of Computational Chemistry*, vol. 30, no. 10, pp. 1545-1614, 2009.
[32] S. Jo *et al.*, "CHARMM-GUI PDB manipulator for advanced modeling and simulations of proteins containing nonstandard residues," *Advances in Protein Chemistry and Structural Biology*, vol. 96, pp. 235-265, 2014. https://doi.org/10.1016/bs.apcsb.2014.06.002
[33] D. R. Roe and T. E. Cheatham III, *Parallelization of CPPTRAJ enables large scale analysis of molecular dynamics trajectory data*. Hoboken, NJ: Wiley Online Library, 2018.
[34] G. A. Gyebi, O. M. Ogunyemi, I. M. Ibrahim, S. O. Afolabi, and J. O. Adebayo, "Dual targeting of cytokine storm and viral replication in COVID-19 by plant-derived steroidal pregnanes: An in silico perspective," *Computers in Biology and Medicine*, vol. 134, p. 104406, 2021.
[35] O. M. Ogunyemi *et al.*, "Dietary stigmastane-type saponins as promising dual-target directed inhibitors of SARS-CoV-2 proteases: A structure-based screening," *RSC Advances*, vol. 11, no. 53, pp. 33380-33398, 2021. https://doi.org/10.1039/D1RA05976A
[36] B. R. Miller III, T. D. McGee Jr, J. M. Swails, N. Homeyer, H. Gohlke, and A. E. Roitberg, "MMPBSA. py: an efficient program for end-state free energy calculations," *Journal of Chemical Theory and Computation*, vol. 8, no. 9, pp. 3314-3321, 2012.
[37] M. S. Valdés-Tresanco, M. E. Valdés-Tresanco, P. A. Valiente, and E. Moreno, "gmx_MMPBSA: a new tool to perform end-state free energy calculations with GROMACS," *Journal of Chemical Theory and Computation*, vol. 17, no. 10, pp. 6281-6291, 2021.
[38] O. A. Ojo *et al.*, "Gongronema latifolium leaf extract modulates hyperglycaemia, inhibits redox imbalance and inflammation in alloxan-induced diabetic nephropathy," *Journal of Diabetes & Metabolic Disorders*, vol. 19, pp. 469-481, 2020. https://doi.org/10.1007/s40200-020-00533-0
[39] R. Hussein and A. El-Anssary, *Plants secondary metabolites: The key drivers of the pharmacological actions of medicinal plants. In B. Builders (Ed.), Herbal medicine*. London, UK: IntechOpen, 2018.
[40] O. Ojo and C. Akintayo CO, "Assessment of antioxidant activity of Ficus asperifolia Miq aqueous extract-In vitro studies," *The Journal of Phytopharmacology*, vol. 3, no. 1, pp. 1-6, 2014. https://doi.org/10.31254/phyto.2014.3103
[41] U. Anand, N. Jacobo-Herrera, A. Altemimi, and N. Lakhssassi, "A comprehensive review on medicinal plants as antimicrobial therapeutics: potential avenues of biocompatible drug discovery," *Metabolites*, vol. 9, no. 11, p. 258, 2019. https://doi.org/10.3390/metabo9110258
[42] O. A. Ojo, P. I. Nwafor-Ezeh, D. E. Rotimi, M. Iyobhebhe, A. D. Ogunlakin, and A. B. Ojo, "Apoptosis, inflammation, and oxidative stress in infertility: A mini review," *Toxicology Reports*, vol. 10, pp. 448-462, 2023. https://doi.org/10.1016/j.toxrep.2023.04.006
[43] O. A. Ojo, A. A. Afon, A. B. Ojo, B. O. Ajiboye, B. E. Oyinloye, and A. P. Kappo, "Inhibitory effects of solvent-partitioned fractions of two Nigerian herbs (Spondias mombin Linn. and Mangifera indica L.) on α-amylase and α-glucosidase," *Antioxidants*, vol. 7, no. 6, p. 73, 2018. https://doi.org/10.3390/antiox7060073
[44] I. Murtaza, O. L. Majeed, G. Sharma, T. A. Raja, and M. Abdin, "Maximum phenylalanine ammonium lyase (PAL) enzyme activity at mid stage of growth imparts highest hypoglycemic property to fenugreek," *Current Trends in Biotechnology and Pharmacy*, vol. 7, pp. 837–846, 2019.
[45] American Diabetes Association, "Standards of medical care in diabetes—2022 abridged for primary care providers," *Clinical Diabetes*, vol. 40, no. 1, pp. 10-38, 2022. https://doi.org/10.2337/cd22-as01
[46] O. Laila, I. Murtaza, M. Abdin, S. Ahmad, T. Raja, and G. Sharma, "Increase in bioactive compounds during germination improves antioxidant and antidiabetic potential of fenugreek seeds," *International Journal of Scientific Progress & Research*, vol. 18, pp. 50–61, 2015.
[47] J. Talabi, S. Adeyemi, S. Awopetu, B. O. Ajiboye, and O. A. Ojo, "Inhibitory effect of aqueous extracts of raw and roasted Sesamum indicum L. seeds on key enzymes linked to type-2 diabetes (α-amylase and α-glycosidase) and Alzheimer's disease (acetylcholinesterase and butyrylcholinesterase)," *Potravinarstvo Slovak Journal of Food Sciences*, vol. 12, no. 1, pp. 337–346, 2018. https://doi.org/10.5219/866

[48] O. M. Salo-Ahen *et al.*, "Molecular dynamics simulations in drug discovery and pharmaceutical development," *Processes*, vol. 9, no. 1, p. 71, 2020.
[49] H. A. Filipe and L. M. Loura, "Molecular dynamics simulations: Advances and applications," *Molecules*, vol. 27, no. 7, p. 2105, 2022.
[50] M. Arnittali, A. N. Rissanou, and V. Harmandaris, "Structure of biomolecules through molecular dynamics simulations," *Procedia Computer Science*, vol. 156, pp. 69-78, 2019.
[51] P. Ferrara, J. Apostolakis, and A. Caflisch, "Evaluation of a fast implicit solvent model for molecular dynamics simulations," *Proteins: Structure, Function, and Bioinformatics*, vol. 46, no. 1, pp. 24-33, 2002.
[52] V. S. Rao and K. Srinivas, "Modern drug discovery process: An in silico approach," *Journal of Bioinformatics and Sequence Analysis*, vol. 2, no. 5, pp. 89-94, 2011.
[53] A. K. Ghose, V. N. Viswanadhan, and J. J. Wendoloski, "A knowledge-based approach in designing combinatorial or medicinal chemistry libraries for drug discovery. 1. A qualitative and quantitative characterization of known drug databases," *Journal of Combinatorial Chemistry*, vol. 1, no. 1, pp. 55-68, 1999.
[54] W. J. Egan, "Predicting ADME properties in drug discovery," *Drug Design: Structure-and Ligand-Based Approaches*, pp. 165-177, 2010.
[55] M. P. Pollastri, "Overview on the Rule of Five," *Current Protocols in Pharmacology*, vol. 49, no. 1, pp. 9.12. 1-9.12. 8, 2010. https://doi.org/10.1002/0471141755.ph0912s49
[56] X. Liu, B. Testa, and A. Fahr, "Lipophilicity and its relationship with passive drug permeation," *Pharmaceutical Research*, vol. 28, no. 5, pp. 962-977, 2011. https://doi.org/10.1007/s11095-010-0303-7
[57] H. Lennernäs, "Intestinal permeability and its relevance for absorption and elimination," *Xenobiotica*, vol. 37, no. 10-11, pp. 1015-1051, 2007. https://doi.org/10.1080/00498250701704819
[58] P. Ertl and A. Schuffenhauer, "Estimation of synthetic accessibility score of drug-like molecules based on molecular complexity and fragment contributions," *Journal of Cheminformatics*, vol. 1, no. 1, p. 8, 2009.
[59] Y. Deng and B. Roux, "Computations of standard binding free energies with molecular dynamics simulations," *The Journal of Physical Chemistry B*, vol. 113, no. 8, pp. 2234-2246, 2009. https://doi.org/10.1021/jp807701h

Edelweiss Applied Science and Technology
ISSN: 2576-8484
Vol. 10, No. 1: 102-127, 2026
DOI: 10.55214/2576-8484.v10i1.11532